



Infant brain probability templates for MRI segmentation and normalization

Mekibib Altaye^{a,*}, Scott K. Holland^a, Marko Wilke^{b,c}, Christian Gaser^d

^a Center for Epidemiology and Biostatistics, Cincinnati Children's Hospital Medical Center, Department of Pediatrics, University of Cincinnati, 3333 Burnet Ave., Cincinnati, OH 45229-3039, USA

^b Department of Pediatric Neurology and Developmental Medicine, Children's Hospital, University of Tübingen, Germany

^c Section for Experimental MR of the CNS, Department of Neuroradiology, University of Tübingen, Germany

^d Department of Psychiatry, University of Jena, Germany

ARTICLE INFO

Article history:

Received 18 April 2008

Revised 29 July 2008

Accepted 31 July 2008

Available online 13 August 2008

ABSTRACT

Spatial normalization and segmentation of infant brain MRI data based on adult or pediatric reference data may not be appropriate due to the developmental differences between the infant input data and the reference data. In this study we have constructed infant templates and *a priori* brain tissue probability maps based on the MR brain image data from 76 infants ranging in age from 9 to 15 months. We employed two processing strategies to construct the infant template and *a priori* data: one processed with and one without using *a priori* data in the segmentation step. Using the templates we constructed, comparisons between the adult templates and the new infant templates are presented. Tissue distribution differences are apparent between the infant and adult template, particularly in the gray matter (GM) maps. The infant *a priori* information classifies brain tissue as GM with higher probability than adult data, at the cost of white matter (WM), which presents with lower probability when compared to adult data. The differences are more pronounced in the frontal regions and in the cingulate gyrus. Similar differences are also observed when the infant data is compared to a pediatric (age 5 to 18) template. The two-pass segmentation approach taken here for infant T1W brain images has provided high quality tissue probability maps for GM, WM, and CSF, in infant brain images. These templates may be used as prior probability distributions for segmentation and normalization; a key to improving the accuracy of these procedures in special populations.

© 2008 Elsevier Inc. All rights reserved.

Introduction

Spatial normalization of individual imaging data to a common reference frame allows us to make statistical inferences across and between groups of individuals. This is usually accomplished by transforming individual image data to a standardized stereotaxic space. Typically, registration and warping of an individual brain into a stereotaxic space is done using a template created from the average of a large number of brain images (Guimond et al., 2000). Talairach and Tournoux described the original method for transforming brain images into a common reference frame based on detailed anatomical measurements in a single individual (Talairach and Tournoux 1988). More recently, the coordinate frame created at the Montreal Neurological Institute (MNI) was constructed from 152 healthy adults between the ages of 18 and 44 years (Evans et al., 1993). However, the use of this template for spatial normalization in special populations such as children, infants and neonates, has been questioned by several authors (Muzik et al., 2000; Burgund et al., 2002; Wilke and Holland, 2003; Hoeksma et al., 2005; Machilsen et al., 2007; Murgasova et al.,

2007). To this end Wilke et al. (2003) created a pediatric template (CCHMC) using brain images from a large number of children between the ages of 5 and 18. They demonstrated the misclassification that can result from using the adult template and prior probabilities for spatial normalization of pediatric data. There have been some attempts to construct an infant template; however, these are based on a very limited number of infants (Dehaene-Lambertz et al., 2002; Srinivasan et al., 2007; Kazemi et al., 2007).

Similarly, in morphological studies based on segmentation of the human brain into different tissue classes, most approaches use *a priori* reference data to improve classification of brain tissue so that classification is not only based upon the input voxel intensity information alone. The recently-proposed unified segmentation framework offered within the SPM5 environment, integrates tissue classification with bias correction and image registration, and it estimates the associated parameters by minimizing the resulting objective function (Ashburner and Friston, 2005). However, if the prior data is taken from an adult reference population, it may not be an appropriate template for data from special populations, such as that from infants.

In this study we set out to construct an infant brain template and associated probability maps for GM, WM and CSF that can be used for registration and as *a priori* information in segmenting new infant brain images. We constructed an infant brain template and *a priori*

* Corresponding author. Fax: +1 513 636 1254.

E-mail addresses: mekibib.altaye@cchmc.org (M. Altaye), scott.holland@cchmc.org (S.K. Holland).

data using high quality T1-weighted 3 Tesla magnetic resonance (MR) images from 76 infants whose age ranged from 9 to 15 months. We utilized the unified segmentation procedure implemented in Statistical Parameter Mapping (SPM5) software (Wellcome Department, University College, London, UK), but modified it to include a Hidden Markov Random Field (HMRF) model as an additional spatial constraint (Cuadra et al., 2005). We also modified the default segmentation procedure provided in SPM5 in order to omit the use of the adult *a priori* data from the tissue probability estimates. The new segmentation algorithm is based on a Gaussian Mixture Model, but in contrast to the SPM5 segmentation (default) algorithm the final tissue probabilities are estimated without tissue priors (Gaser et al., 2007). In an effort to further reduce the impact of the adult prior data, we employed a *two-pass approach*. In the first pass the adult *a priori* data are used. Then in the second pass, the infant probability data generated by the first pass approach are used.

After constructing infant brain image templates and tissue probability maps using the new methods, we quantified the magnitude of differences between the newly constructed infant population data and MNI adult reference data or CCHMC pediatric reference data. Quantitative comparisons are summarized in Table 2 for convenience.

Materials and methods

Subjects

Our subjects were drawn from two different, currently ongoing protocols. The first protocol is testing fMRI of auditory language stimulation in hearing-impaired infants at or near 12 months of age. Infants with normal hearing and hearing impairment were recruited to compare fMRI results with auditory and speech stimulation between the two groups. This protocol is designed to test whether fMRI of auditory language stimulation in a hearing-impaired infant can provide specific, clinically relevant details about the child's auditory perception and processing ability. Specifically infants between the ages of 9 and 15 months (12 ± 3) were included in the protocol, and currently data for 28 (9 male and 19 female) hearing-impaired and normal hearing control subjects is available for processing.

In order to increase the number of subjects for the template construction we include additional infants from a second protocol. This protocol includes infants referred for clinical brain imaging with MRI for clinical diagnosis of various indications. From this protocol, forty nine infants (22 male and 27 female; age range 9–15 months) were found to have normal brain anatomy, confirmed by the attending neuroradiologist at the time of scan. They were thus included in the current study.

Overall, MR images from 77 infants (46 female and 31 male) aged between 9 and 15 months, were acquired from sedated infants being scanned for clinical indications as described above. Imaging data from one 9 month old female infant was excluded, as image artifacts interfered with the segmentation procedure. The remaining 76 MR images were visually confirmed to be free of artifacts and were thus used for all subsequent analyses. The age distribution of the resulting 76 infants (45 female and 31 male) is presented in Table 1. Infants in both protocols were sedated using either chloral hydrate 75 mg/kg or Nembutal 5 mg/kg. Institutional Review Board approval was obtained for this study which involves retrospective data analysis.

Data acquisition and preparation

Infants were imaged with a clinical 3 Tesla clinical MRI Scanner (Siemens Trio, Siemens Medizintechnik, Erlangen, Germany). High resolution T1-weighted, 3D brain images were acquired using the Magnetization Prepared Rapid Acquisition Gradient Echo (MPRAGE)

Table 1
Age and gender distribution of the study population

Age (months)	Gender		Total
	Female	Male	
9	6	8	14
10	5	2	7
11	7	5	12
12	7	7	14
13	7	3	10
14	10	2	12
15	3	4	7
Total	45	31	76

method (Mugler and Brookeman, 1990). The imaging parameters used were TR=2000 ms, TE=2.93 ms for $n=68$ subjects, and TR=1900 ms, TE=4.13 ms for $n=8$ subjects; flip angle = 12° , FOV $15 \times 20 \times 19.2$ cm and matrix $[208-512] \times [256-512] \times [128-192]$ resolution. All data was imported from DICOM format into ANALYZE format for analysis using the SPM5 DICOM import function. All processing was done using SPM5 or stand-alone scripts running in MATLAB. Instead of manually orienting the data using the display option in SPM5, an automated center of mass approach was used.

Processing: template and *a priori* data construction

Our objective was to construct an infant template and *a priori* data that can be used for improved spatial normalization and the morphological study of infant data. In order to achieve this we employed two different processing strategies. The first strategy uses the standard unified segmentation approach that utilizes adult *a priori* data for segmentation. This is the default strategy in SPM5, though we modified it to incorporate the HMRF model to additionally introduce spatial constraint. This modification to the algorithm helps in determining the probability of a given voxel to belong to a tissue class which is achieved by calculating the MRF energy for a given voxel, based on its proximity to the surrounding voxels. The unified segmentation approach in SPM5 finds a Maximum a Posteriori (MAP) solution by repeatedly alternating among classification, bias correction and registration steps in a unified generative model involving a mixture of Gaussians, bias correction component and warping (non-linear registration) component (Ashburner and Friston, 2005). This process is indicated by the segmentation engine diagrammed in Fig. 1. This strategy will be referred to as the *default strategy* for the rest of the paper. The second processing strategy, basing segmentation solely on current voxel intensity and not using prior information, has only recently been implemented as a custom function within the unified segmentation approach in SPM5. The segmentation is based on a Gaussian mixture model and the final tissue probabilities are estimated without tissue priors. We additionally applied the HMRF model to introduce spatial constraints (Cuadra et al., 2005). This strategy will be referred to as *the new strategy* for the rest of the paper. A flow chart outlining both strategies is diagrammed in Fig. 1.

Each strategy was deployed using two different approaches, where first we established a first pass template and *a priori* data based on the adult or pediatric reference data. These templates are then used in a second iteration as reference data to yield a second pass template and *a priori* data. To clarify the two strategies combined with two approaches employed and the comparisons resulting from these combinations, a flow chart is provided in Fig. 1.

For all processing strategies and approaches, a light cleaning procedure within the SPM5 segmentation procedure was used in order to remove residual non-brain tissue from the segmented images. All normalized data are written out with the same resolution and dimension ($157 \times 189 \times 156$ voxels at $1 \times 1 \times 1$ mm resolution) and, then averaged to create *a priori* probability maps of GM, WM and CSF.

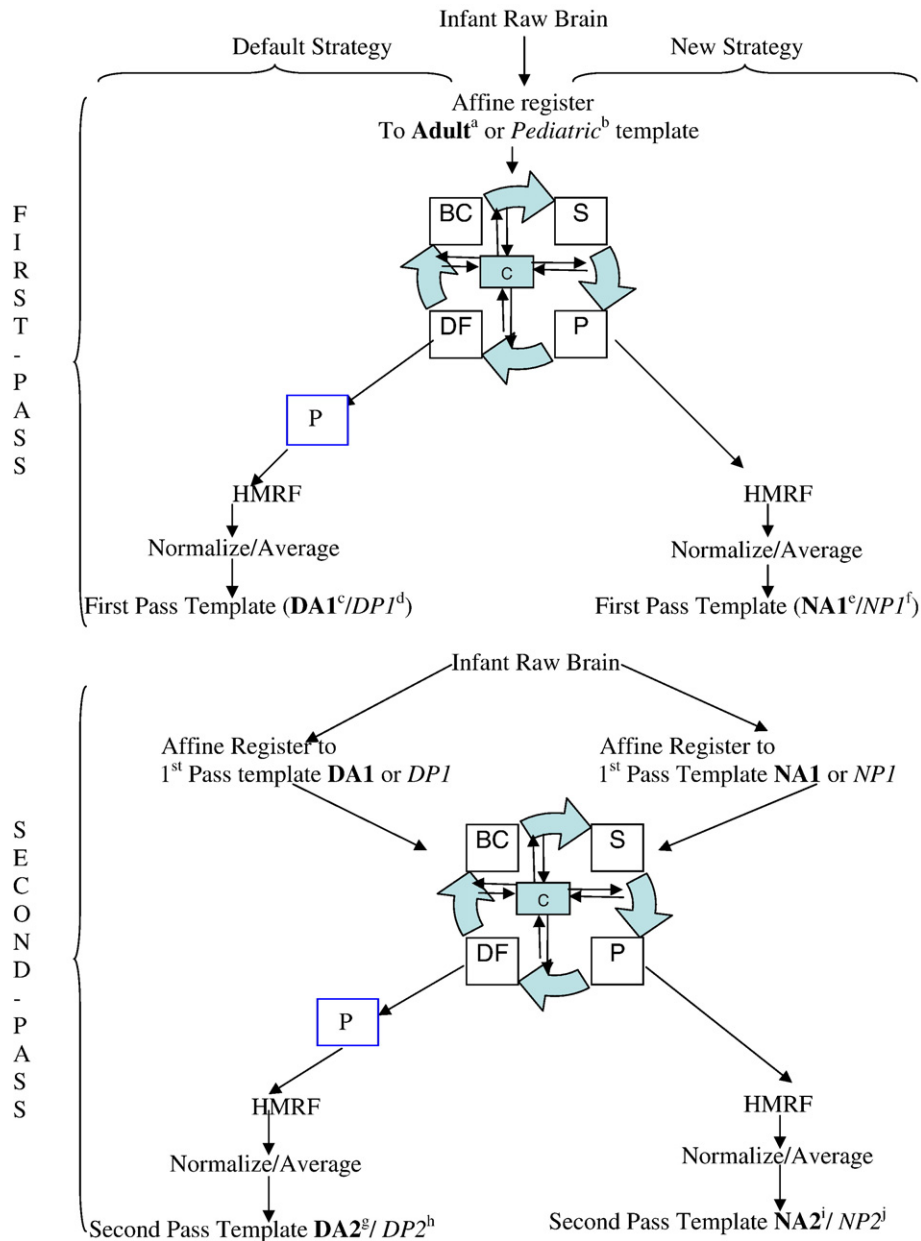


Fig. 1. Overview of infant template construction. Initially all images are registered to the adult/pediatric template. After registration a segmentation estimation procedure is used to estimate the parameters by iteratively going through segmentation (S), bias correction (BC), deformation (DF) and priors (P) until convergence criteria (C) are met. After this step two strategies are used for calculation of the tissue probability maps. The first (default) strategy includes adult prior probabilities for distribution of GM, WM and CSF based on adult/pediatric data indicated by the inclusion of the blue box (P). The second (new) strategy does not use prior probability distributions in the calculation of the tissue probability maps; instead it only uses the intensity of the T1 images. Then a Hidden Markov Random Field (HMRF) process is applied to the resulting image, normalized and averaged to produce the first pass template. Second pass templates are obtained in similar fashion except the first pass template is used for registration and normalization. Key: DA1/DPI = First pass adult/pediatric template via default strategy; DA2/DP2 = Second pass adult/pediatric template via default strategy; NA1/NPI = First pass adult/pediatric template via new strategy; NA2/NP2 = Second pass adult/pediatric template via new strategy. Bold font indicates adult data while italic font indicates pediatric data. Comparisons: 1. (g-a) and (i-a); 2. (h-b) and (j-b); 3. (g-i); 4. (g-c), (i-e) and (h-d), (j-f); using number conventions from Table 2.

Similarly, we applied the normalization parameters obtained from the segmentation step to write out each individual normalized T1-weighted image and calculated the average of all normalized T1-images (Fig. 2).

Assessment of differences

Comparison with adult and pediatric reference data

The first round of comparison (comparison 1, Table 2) involves data obtained from the two processing strategies against the default SPM5 adult *a priori* data. The adult data is based on the scans of 152 young, healthy subjects from Montreal Neurological Institute (MNI-152). The

second round of comparison (comparison 2, Table 2) uses data obtained from the two processing strategies against the pediatric *a priori* data. The pediatric data is based on 200 healthy children between the ages of 5 and 18 years, and is provided by Cincinnati Children's Hospital Medical Center (CCHMC2-200), available at www.irc.cchmc.org/software/pedbrain.php. An outline of the comparison strategies is presented in Table 2.

Comparison between processing strategies and approaches

In addition to these comparisons we also assessed the impact on the infant template and the corresponding infant *a priori* data images resulting from the two processing strategies (comparison 3, Table 2).

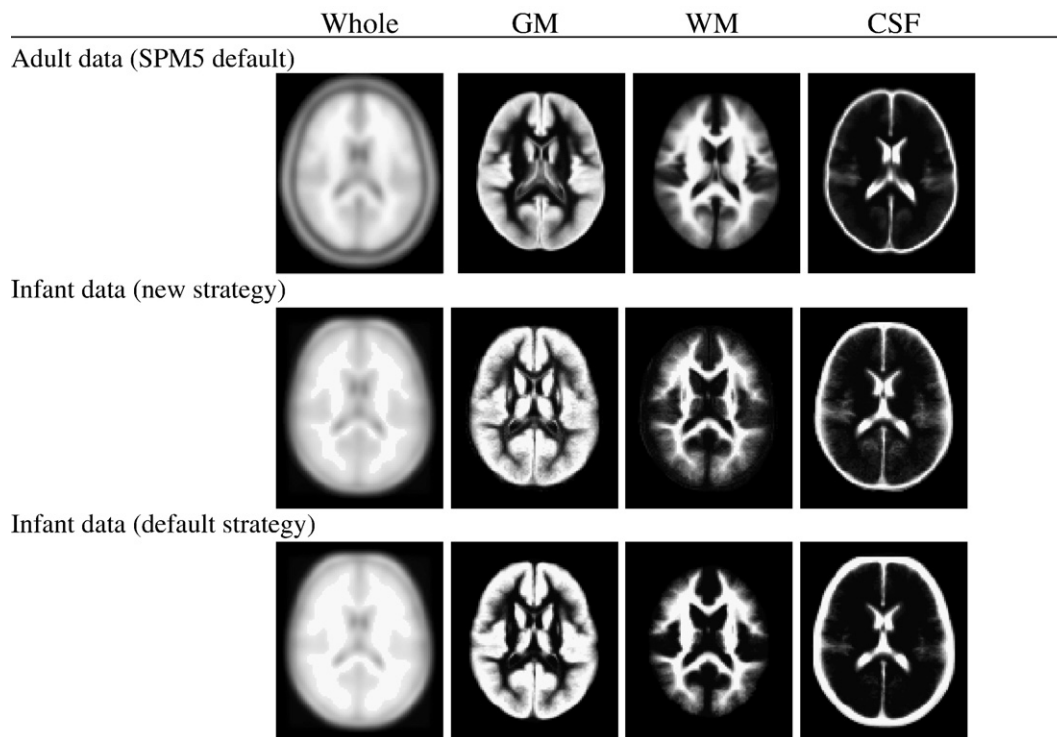


Fig. 2. Display of adult reference data and infant templates including GM, WM and CSF probability maps. The top panel is for the adult data (SPM 5 default), the middle panel is for infant data processed using the new strategy and the bottom panel is for infant data processed using the default strategy as outlined in Fig. 1. The displayed infant data is based on second pass output.

Using this comparison we are able to evaluate the impact of the use of adult prior data in the resulting images. We also compared the images obtained from the two approaches used for each strategy. Specifically the difference between first pass (use of adult data) and second pass (use of infant data) data are compared (comparison 4, Table 2).

We used the SPM image calculation function to calculate the differences between pairs of images. We displayed the difference between two images using MRICro with color coding, where red and yellow indicated higher tissue concentration in the infant data (i.e. infant > adult, or infant > pediatric) and blue indicated lower tissue concentration in the infant data (infant < adult, or infant < pediatric). Only tissue probability differences of at least 20% are displayed in the color overlays (Figs. 3 and 4). All results are in neurological orientation. We also display these differences using a histogram, illustrating the distribution of these differences. The histograms are obtained by retaining voxels from the difference image that are greater than 0.2 and less than -0.2. Only tissue probability differences of 20% or more (i.e. differences in tissue probabilities that are >0.2 or <-0.2) are plotted in the histograms in Figs. 3–6. The percentage of voxels classified consistently (within the 20% limit) or inconsistently between the strategies and approaches are also indicated in the figures.

Results

All processing strategies, including the use of adult *a priori* data as a reference template for registration and segmentation, produce high quality images as displayed in Fig. 2. However there are significant differences in tissue classifications between the newly created infant and the adult (Fig. 3) as well the infant and pediatric (Fig. 4) GM, WM and CSF tissue probability maps in both strategies employed here. The degree of discordance seems to be higher when the default strategy is used (via the default SPM5 segmentation routine) to generate the resulting infant data. In general the results show that in the infant reference data, brain tissues tend to be classified as GM with higher

probability compared to adult reference data (Fig. 3) and to a lesser extent with pediatric reference data (Fig. 4), as indicated by the red and yellow colors.

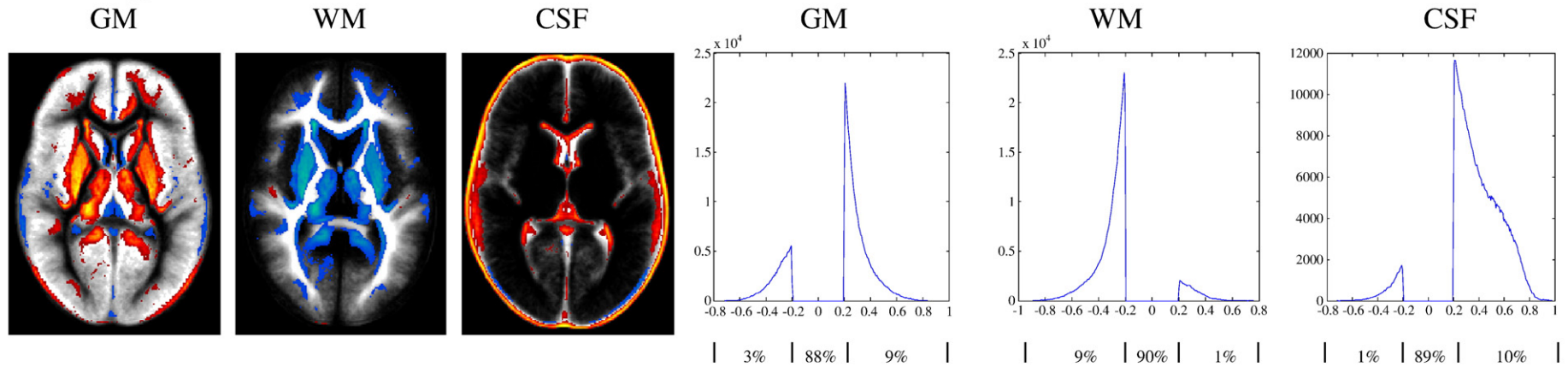
However this seems to occur at the expense of WM, which is presented with higher probability in both the adult and pediatric reference data as indicated by the blue color. With infant data generated using the new strategy versus adult reference data, GM is classified with greater probability at the superior frontal gyrus, medial frontal gyrus, anterior cingulate, putamen, and thalamus as shown in Fig. 3 (top). In addition to these areas, comparison of infant data obtained using the default strategy versus the adult reference data results in additional pixels in the inferior frontal gyrus, middle

Table 2
Summary of the different comparisons made

Comparison	Image 1	Image 2	Differences
1	New Infant GM/WM/CSF constructed under the new and default strategies. (Initial registration was with adult reference data). (i) and (g)	Adult prior GM/WM/CSF (a)	Fig. 3
2	New Infant GM/WM/CSF constructed under the new and default strategies. (Initial registration was with pediatric reference data). (j) and (h)	Pediatric prior GM/WM/CSF (b)	Fig. 4
3	New infant GM/WM/CSF constructed under the new strategy (i)	New infant GM/WM/CSF constructed under the default strategy (g)	Fig. 5
4	First pass infant GM/WM/CSF constructed under both strategies (e) and (c)	Second pass infant GM/WM/CSF constructed under both strategies (i) and (g)	Fig. 6

Except for comparison 4, all comparisons are based on second pass images. Bold letters indicate image reference to Fig. 1.

New strategy versus adult reference data



Default strategy versus adult reference data

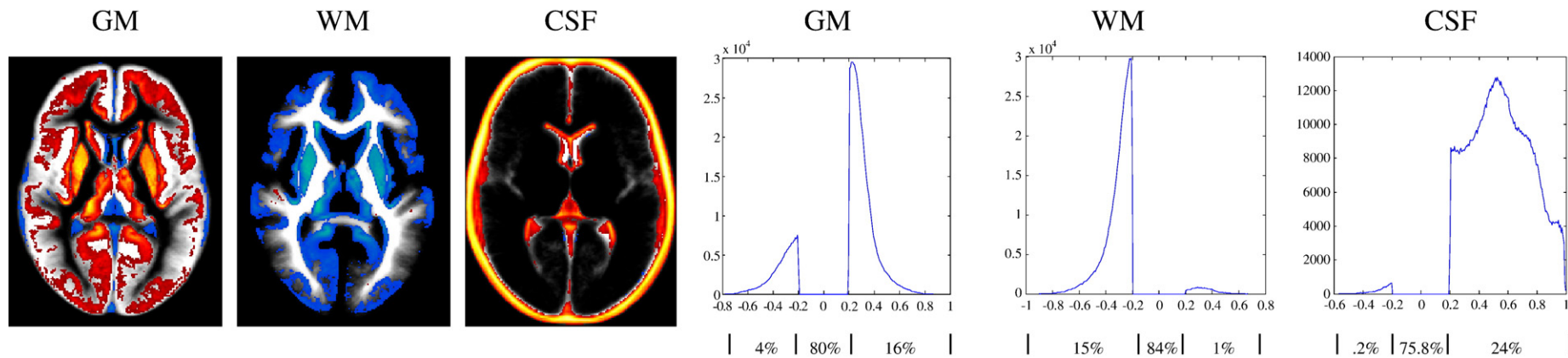
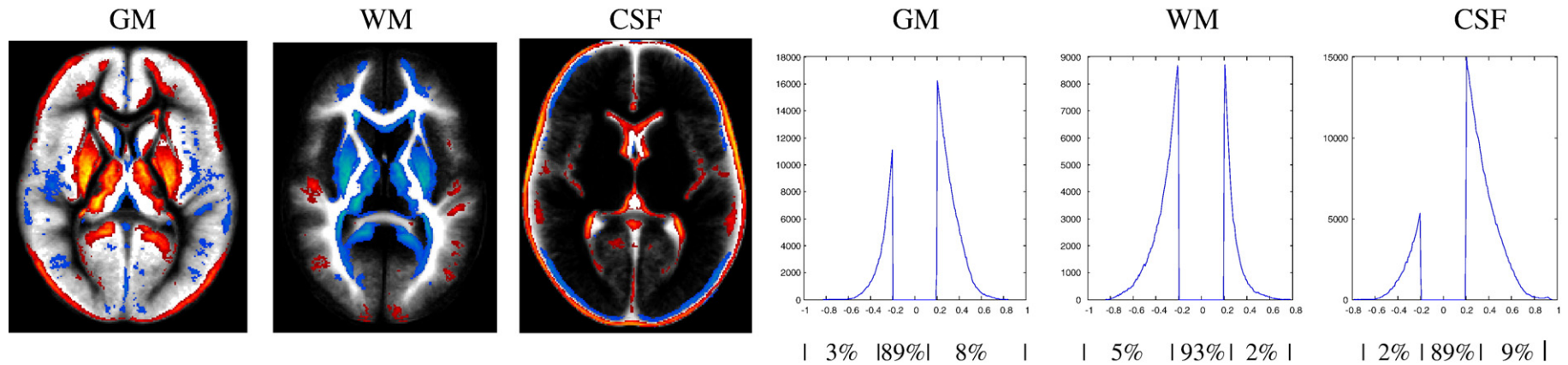


Fig. 3. Comparison of adult *a priori* data and infant GM, WM and CSF distributions constructed using the new (top panel) and default (bottom panel) strategies as outlined in Fig. 1. Differences are displayed as an overlay on the infant data to show spatial location (left panels, where red and yellow indicates infant probability is greater than adult probability while blue is for the reverse effect), and as a histogram to show their distribution (right panels). Results shown are for differences of at least 20% in tissue probability and are based on the second pass output. For the histograms, the x-axis represents the magnitude of differences and the y-axis the corresponding number of voxels. The flat line between -0.2 and 0.2 indicates the 20% threshold used, while the curves on the right and left indicate where the infant tissue probability is greater or less than the adult data respectively. Percentages of voxels in each segment of the histogram (i.e. <-0.2, no difference, >0.2) are listed below the horizontal axis.

New strategy versus pediatric reference data



Default strategy versus pediatric reference data

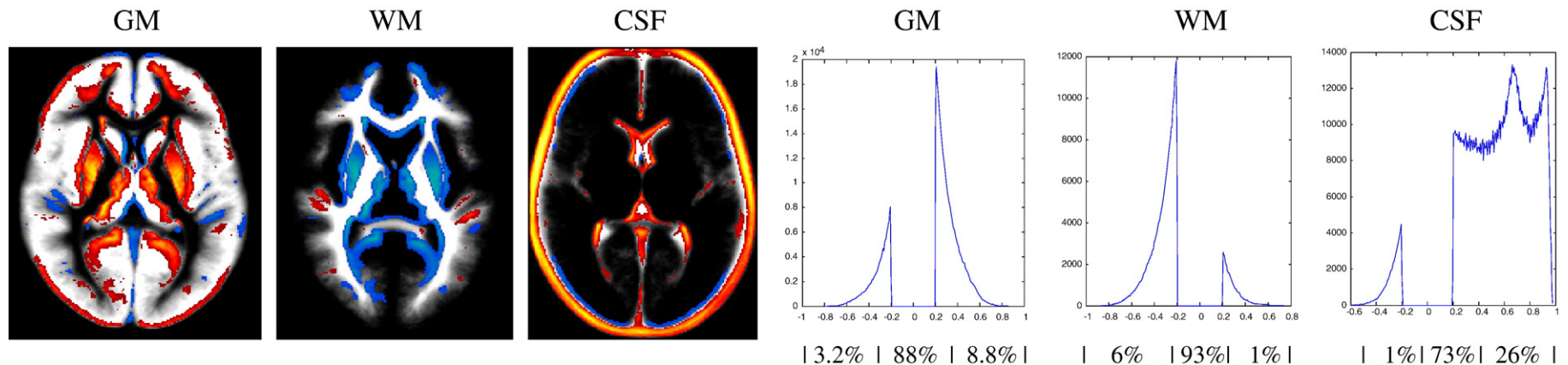
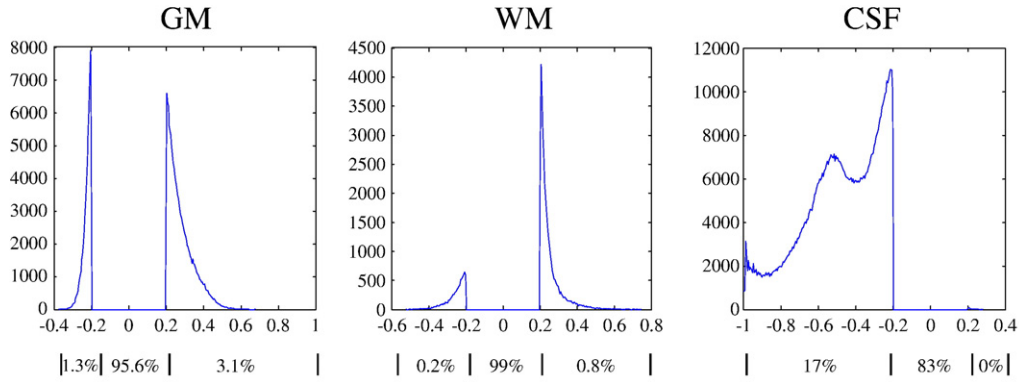


Fig. 4. Comparison of pediatric *a priori* data versus infant GM, WM and CSF distributions constructed using new (top panel) and default (bottom panel) strategies as outlined in Fig. 1. Differences are displayed as an overlay on the infant data to show spatial location (left panels, where red and yellow indicates infant probability is greater than pediatric probability while blue is for the reverse effect), and as a histogram to show their distribution (right panels). Results shown are for differences of at least 20% in tissue probability and are based on the second pass output. For the histograms, the x-axis represents the magnitude of differences and the y-axis the corresponding number of voxels. The flat line between -0.2 and 0.2 indicates the 20% threshold used, while the curves on the right and left indicate where the infant tissue probability is greater or less than the pediatric data respectively. Percentages of voxels in each segment of the histogram (i.e. <-0.2 , no difference, >0.2) are listed below the horizontal axis.

New strategy versus Default strategy (adult reference data used for initial registration)



New strategy versus Default strategy (pediatric reference data used for initial registration)

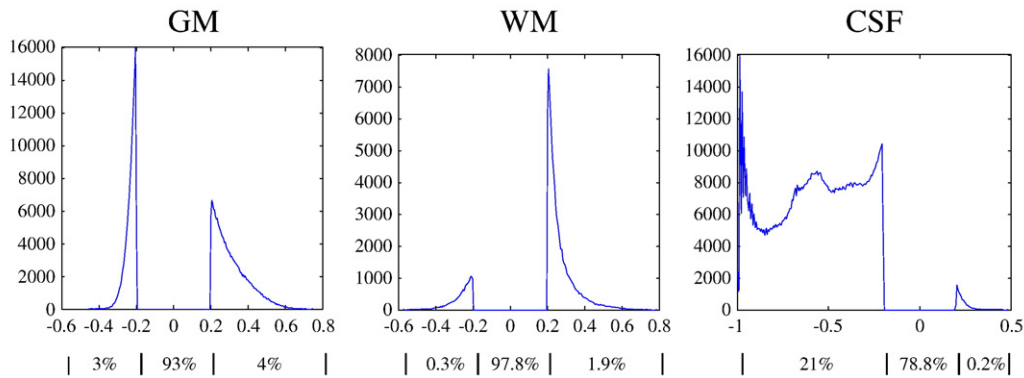


Fig. 5. Comparison of GM, WM and CSF probability distributions in second pass infant data obtained with the new and default strategy. In the top panel adult and in the bottom pediatric reference data were used for initial registration. The histograms indicate the distribution of the differences for each tissue class. Results shown are for differences of at least 20% in tissue probability. For the histograms, the x-axis represents the magnitude of differences and the y-axis the corresponding number of voxels. The flat line between -0.2 and 0.2 indicates the 20% threshold used, while the curves on the right and left indicate where the infant tissue probability obtained using the new strategy is greater or less than the infant data obtained using the default strategy respectively. Percentages of voxels in each segment of the histogram (i.e. <-0.2, no difference, >0.2) are listed below the horizontal axis.

occipital gyrus and superior frontal gyrus classified as GM with a higher probability: Fig. 3 (bottom).

We also used the proportion of voxels that showed a difference of 20% or more in classification probability, to additionally quantify the graphically depicted data shown in Figs. 3 and 4 (left panel). These proportions are calculated by counting the number of voxels that are below -0.2 or above 0.2 (20% threshold rule) and dividing it by the total number of voxel in the tissue under consideration (4.6 million pixels). Each histogram shown in Figs. 3 to 6 is divided into three distinct areas. The left and right “bumps” represent the proportion of voxels that are below -0.2 and above 0.2 respectively when looking at the distribution of the difference of the two images considered. The middle section between (± 0.2) corresponds to the proportion of voxels that are classified consistently by both methods, according to the 20% threshold rule used in this paper. The proportion of voxels in each segment of the histogram is indicated below the horizontal axis of Figs. 3–6. The sum of the proportion in the three areas should add to 1.

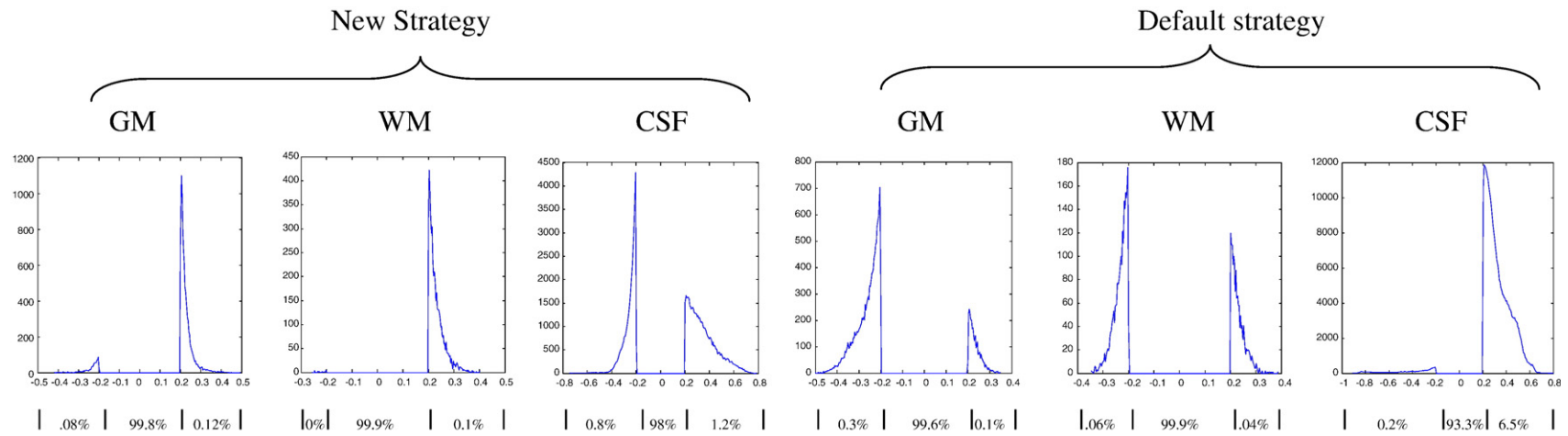
Additionally, if one strategy or approach causes voxels to misclassify as one tissue class (for example GM) then we expect an equivalent number of voxels to be lost from the rest of the tissue classes combined (for example WM+CSF). However in our case since we used a 20% threshold rule the numbers may not always balance out because some voxels may also be shifted in and out of the 20% threshold group. For example in Fig. 3 (right top panel) the proportion of voxels that are misclassified as high for GM is 9%, while the proportion of voxels that are misclassified as low for the combined WM and CSF is 10% (9%+1%). Although close the proportions are not

exactly the same, this is because 1% of the voxels classified as high for GM shifts into the concordant classification group.

When we compare the newly created infant GM, WM and CSF using the new strategy with the corresponding adult reference data: Fig. 3 (top) the proportion of voxels that showed a difference of 20% or more were 12%, 10% and 11% for GM, WM and CSF respectively. The magnitude of these proportions increases to 20%, 16%, and 24.2% when the infant data is constructed using the default strategy: Fig. 3 (bottom). This indicates that the use of adult *a priori* data in the segmentation step, as is the case for the default strategy, increases the number of discordant (beyond 20% difference in probability) voxels. Among the voxels that show a difference of 20% or more, the proportion of voxels that the newly constructed infant data classifies with higher probability, were 75%, 10% and 91% for GM, WM and CSF respectively when the data is obtained using the new strategy. These proportions were 80%, 6.2% and 99% when the comparison infant data was created with the default strategy. These distributions are displayed on the right panel of Fig. 3. This shows that the newly created infant data classifies GM and CSF with higher probability but at the expense of WM which was classified with lower probability.

Similar patterns were observed when we compare the newly created infant data with the corresponding pediatric reference data. When comparing the infant data created using the new strategy with the pediatric reference data, the proportions of voxels that show a difference of 20% or more in classification probability were 11%, 7% and 11% for GM, WM and CSF respectively: Fig. 4 (top). These proportions were 11%, 7% and 27% when the infant data was constructed using the default strategy: Fig. 4 (bottom). Unlike the comparison of the infant

First pass vs second pass (adult reference data used for initial registration)



First pass vs second pass (pediatric reference data used for initial registration)

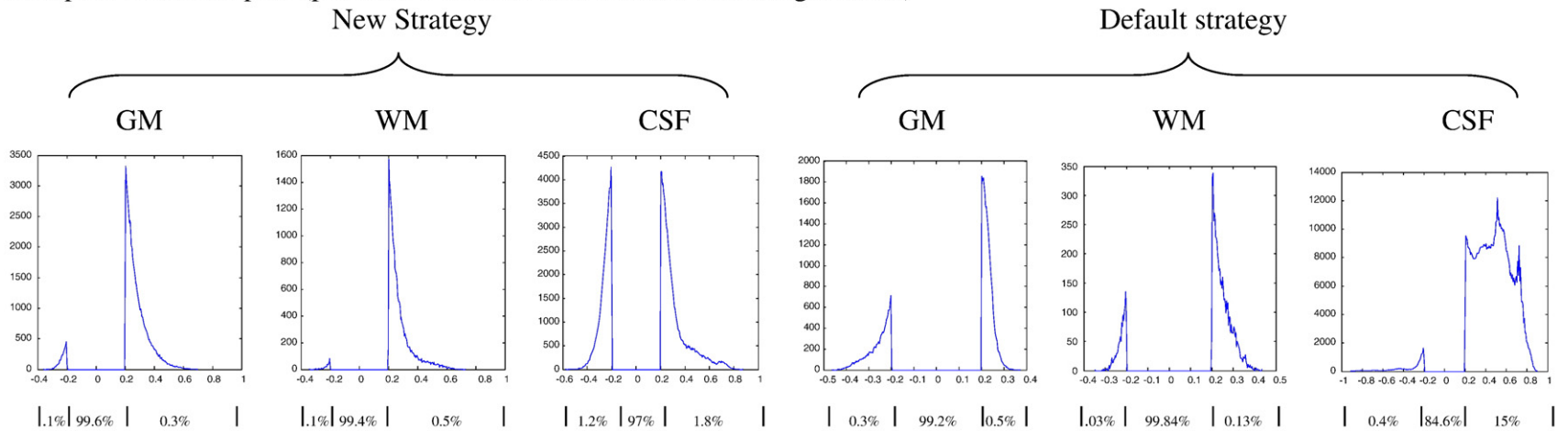


Fig. 6. Comparison of first pass and second pass probability maps for images prepared using the new (left panel) and default (right panel) strategies, for adult (top panel) and pediatric (bottom panel) reference data. The histograms show the distribution of these differences for each tissue class and strategy. Results shown are for differences of at least 20% in tissue probability. The x-axis represents the magnitude of differences and the y-axis the corresponding number of voxels. The flat line between -0.2 and 0.2 indicates the 20% threshold used, while the curves on the right and left indicate where the infant tissue probability obtained using the second pass approach is greater or less than the infant data obtained from the first pass approach respectively. Percentages of voxels in each segment of the histogram (i.e. <-0.2 , no difference, >0.2) are listed below the horizontal axis.

data with the adult reference data, where the use of the default strategy increased the proportion of voxels that shows a difference of 20% or more; here the proportions are very similar (except for CSF) for both strategies used. In addition the proportion of voxels classified with high probability as GM, WM, and CSF in the second pass infant data that is constructed using the new strategy are 72%, 28.6% and 81.8% respectively. These proportions were 72.7%, 14.3% and 96% when the infant data was constructed using the default strategy. These distributions are displayed in the right panel of Fig. 4.

The comparisons between the images obtained using the new and the default strategy resulted in similar images with only moderate differences as defined here. The proportion of voxels that show a difference of 20% or more between the images resulted from the two strategies where adult reference data was used for initial registration (Fig. 1: DA2 and NA2), were 4.4%, 1% and 17% for GM, WM and CSF respectively (Fig. 5: top). Similar but consistently greater differences were observed when comparing the newly created infant data using the two strategies where the initial registration was based on pediatric reference data (Fig. 1: DP2 AND NP2). In this case the proportions of voxels that differ by more than 20% were 7%, 2.2% and 21.2% for GM, WM and CSF respectively (Fig. 5: bottom).

The two-pass approach we employed to minimize the impact of the adult prior data results in similar tissue classification in the final infant templates, with very little difference between the images obtained using the two approaches as shown in Fig. 6. The proportion of voxels that show a difference of 20% or more were less than 1% for both GM and WM regardless of the strategy used to generate the infant data when the initial registration were with adult data. However 2% of voxels showed a difference of 20% or more for CSF probability, when the infant data is constructed using the new strategy and 6.7% of voxels when using the default strategy (Fig. 6: top).

Similar patterns but with slightly higher percentages of discordant voxels were observed when the first pass and second pass approaches were compared for images generated using the pediatric reference data for initial registration. Regardless of the strategy used to generate the infant images, the proportions of voxels that exhibit 20% or greater differences were less than 1% for both GM and WM. However for CSF these proportions were 3% when infant data is generated under the new strategy and 15.4% under the default strategy (Fig. 6: bottom).

Discussion

In this article, we present a procedure to create an infant template and *a priori* probability maps of GM, WM and CSF. We used a novel approach that does not require the use of prior data for segmenting brain images in an effort to reduce the impact of inappropriate adult or pediatric prior data. We showed that the use of the default adult or pediatric template to segment the infant data will result in misclassifications of infant tissue, as shown in Figs. 3 and 4. This is consistent with the findings reported when comparing the use of adult *a priori* data for segmenting pediatric data (Wilke et al., 2003) and is likely due to the different shape and size of developing infant brains as well as different GM/WM ratios in the infant brain relative to children and adults.

The observed difference between the newly created infant data and the pediatric reference data (Fig. 1: h-b and j-b) is less severe compared to the difference between the infant and adult reference data (Fig. 1: g-a and i-a) as indicated by the proportion of discordant voxels, particularly when the default strategy was used to generate the infant data (Fig. 1: h-b and g-a). However, the appearance of the observed discordance between the infant and pediatric data mimicked the difference observed between the infant and adult data suggesting that the pediatric data is closer to the adult data in tissue distribution than to the infant data (Figs. 3 and 4). This is apparent when we recognize that the proportion of voxels classified

with high probability in the second pass infant data are very similar whether adult or pediatric reference data were used for initial registration (Fig. 1: g-a and h-b: i-a and j-b). This is depicted in the right panel of Figs. 3 and 4.

The indirect comparison between the two processing strategies through their comparison with the adult reference data as shown in Fig. 3, suggests that the use of the default strategy results in a higher number of discordant voxel classifications than the new strategy. This difference is more precisely depicted in the direct comparison of images obtained from the two strategies as displayed on Fig. 5. This suggests that the new strategy with less discordant voxels may provide more consistent classification for infant brain image data.

However, regardless of the strategy employed to obtain the infant template, our results demonstrate the importance of using appropriately constructed infant templates for future normalization and segmentation of infant images, since the alternative of using adult or pediatric templates will result in misclassification of tissue class as shown in Figs. 3 and 4.

The comparison between images produced using first pass (using adult data) and second pass (using the resulting infant data from first pass procedure) images shows very little difference (Fig. 6). This is likely due to the fact that the priors are warped to the input data during the first pass, so that the influence of the priors is diminished in final images. In addition the use of affine and non-linear transformation in both approaches (first and second pass) coupled with the introduction of the HMRF model, to apply spatial constraints from neighboring voxels, might further reduce the impact of the adult prior data during the first pass segmentation step.

Limitations

The MR data is obtained from infants sedated by either chloral hydrate or Nembutal. The impact of the sedation, if any, on the resulting MR images is unknown. Although unlikely, it is possible that the sedation might have an impact on T1 image intensity distribution and the resulting template and probability maps through either a direct effect or indirectly due to alterations in cerebral perfusion induced by the drugs.

The purpose of spatial normalization is to be able to compare brain activations or structural changes across individuals, which will always entail deforming the contributing subjects to a common spatial reference frame. Comparing the activation patterns from children and adults and finding the evolution that takes place in childhood is only possible if a common reference frame is used for the subjects being compared. Considering the advantages that such a common spatial frame offers over myriads of study-specific custom reference frames, we opted to use the most commonly-used reference frame for our study here (MNI-152). While this choice is arguable, we still believe that the advantages outweigh the disadvantages at this point.

The original study that motivated construction of the template and probability maps using the new methods reported here focused on infants at nominally 12 months of age (± 3 months) as described above in the Materials and methods: Subjects section. So for our purposes, the age span of infants selected for template construction matches our population exactly. However, even this extremely narrow age range might be too wide to preserve fine scale changes over this 6 month period of rapid brain development (Huttenlocher, 1979). Also, the applicability of the specific template and probability maps we offer may be limited to other studies of 1 year olds. The methods described here provide potential users with a completely general formula to construct their own prior-free, templates as needed. In this context, our specific data set is just an example of the power of the new method. For readers who may find it helpful to use our template directly we have made it available on our website at <http://www.irc.cchmc.org/software>.

Conclusion

In the absence of a gold standard, a direct comparison between the proposed new procedure and the default procedure may not establish which procedure is more accurate. However the comparison presented here of the new and default procedure with *a priori* reference data from adults or children, suggests that the new procedure is superior for use in segmentation of infant brain images as it results in less severe misclassification when compared to the default procedure using adult *a priori* probability maps. The new infant template and *a priori* data obtained from the new procedure is therefore recommended for use as a reference data for spatial normalization and segmentation of infant brain MRI data.

Acknowledgments

This work was partially supported by the National Institute of Deafness and Communication Disorders (RO1-DC07186).

References

- Ashburner, J., Friston, K.J., 2005. Unified segmentation. *NeuroImage* 26, 839–851.
- Burgund, E.D., Kang, H.C., Kelly, J.E., Buckner, R.L., Snyder, A.Z., Petersen, S.E., Schlaggar, B.L., 2002. The feasibility of a common stereotactic space for children and adults in fMRI studies of development. *NeuroImage* 17, 184–200.
- Cuadra, M.B., Cammoun, L., Butz, T., Cuisenaire, O., Thiran, J.P., 2005. Comparison and validation of tissue modelization and statistical classification methods in T1-weighted MR brain images. *IEEE Trans Med Imaging* 24, 1548–1565.
- Dehaene-Lambertz, G., Dehaene, S., Hertz-Pannier, L., 2002. Functional neuroimaging of speech perception in infants. *Science* 298, 2013–2015.
- Evans, A.C., Collins, D.L., Mills, S.R., Brown, E.D., Kelly, R.L., Peters, T.M., 1993. 3D statistical neuroanatomical models from 305 MRI volumes. *Proc. IEEE-Nucl Sci Symp Med Imaging Conf* 1813–1817.
- Gaser, C., Altaye, M., Wilke, M., Holland, S.K., 2007. Unified segmentation without tissue priors. *NeuroImage* 36 (Suppl. 1), S68.
- Guimond, A., Meunier, J., Thirion, J.P., 2000. Average brain models: a convergence study. *Comput Vis Image Underst* 77 (2), 192–210.
- Hoeksma, M.R., Kenemans, J.L., Kemner, C., Van Engeland, H., 2005. Variability in spatial normalization of pediatric and adult brain images. *Clin Neurophysiol* 116, 1188–1194.
- Huttenlocher, P., 1979. Synaptic density in human frontal cortex — developmental changes and effects of age. *Brain Res* 163, 195–205.
- Kazemi, K., Moghaddam, H.A., Grebe, R., Gondry-Jouet, C., Wallois, F., 2007. A neonatal atlas template for spatial normalization of whole-brain magnetic resonance images of newborns: preliminary results. *NeuroImage* 37, 463–473.
- Machilsen, B., D'Agostino, E., Maes, F., Vandermeulen, D., Hahn, H.K., Lagae, L., Stiers, P., 2007. Linear normalization of MR brain images in pediatric patients with periventricular leukomalacia. *NeuroImage* 35, 686–697.
- Mugler, J.P., Brookeman, J.R., 1990. Three-dimensional magnetization-prepared rapid gradient-echo imaging (3D MP RAGE). *Magn Reson Med* 15, 152–157.
- Murgasova, M., Dyet, L., Edwards, D., Rutherford, M., Hajnal, J.V., Rueckert, D., 2007. Segmentation of brain MRI in young children. *Academic Radiology* 14, 1350–1366.
- Muzik, O., Chugani, D.C., Juhász, C., Shen, C., Chugani, H.T., 2000. Statistical parametric mapping: assessment of application in children. *NeuroImage* 12, 538–549.
- Srinivasan, L., Dutta, R., Counsell, S.J., Allsop, J.M., Boradman, J.P., Rutherford, M.A., Edwards, A.D., 2007. Quantification of deep gray matter in preterm infants at term-equivalent age using manual volumetry of 3-Tesla magnetic resonance images. *Pediatrics* 119, 759–765.
- Talairach, J., Tournoux, P., 1988. *Co-planar Stereotaxic Atlas of the Human Brain*. Thieme, Stuttgart, Germany.
- Wilke, M., Holland, S.K., 2003. Variability of gray and white matter during normal development: a voxel-based MRI analysis. *Neuroreport* 14, 1887–1890.
- Wilke, M., Schmithorst, V.J., Holland, S.K., 2003. Normative pediatric brain data for spatial normalization and segmentation differs from standard adult data. *Magn Reson Med* 50, 749–757.